

Thermal transport of a delta-doped multilayer with strongly correlated electrons

Veljko Zlatić and James K. Freericks

Abstract We present a theory for the charge and heat transport in a multilayer made of three sets of planes with strongly correlated electrons. The Mott insulator planes make the left and right barrier; a few delta-doped planes which are close to the metal-insulator transition make a conduction channel. In such a device, the currents can only flow parallel to the interfaces. The electron dynamics is described by the Falicov-Kimball model which can be solved for arbitrary large on-site correlation with an inhomogeneous DMFT algorithm. The charge reconstruction induced by the interfaces is taken into account by solving the Poisson equation. We derive the current density operators of the model and compute the thermoelectric coefficients by linear response theory. By tuning the number of electrons in the conducting channel we bring the chemical potential in the a region where the renormalized transport density of states is very steep. This enhances the thermoelectric performance of the device. The results are illustrated by showing the reconstructed charge profile, transport density of states, the electrical resistance, the Seebeck coefficient, the Lorenz number, and the figure-of-merit.

1 Introduction

Thermoelectric materials are attracting a lot of recent attention, because of their potential for various applications and for so-called green technologies. The thermoelectric devices directly convert the thermal energy into electrical energy or vice versa. They are represented schematically in Fig. 1, where two thermal reservoirs at different temperature and voltage are connected by two arms made of a p -type and

V. Zlatić
Institute of Physics, HR-10000 Zagreb, Croatia e-mail: zlatic@ifs.hr

J. K. Freericks
Department of Physics, Georgetown University, Washington D.C., 20057, USA e-mail: freericks@physics.georgetown.edu

n -type semiconductors. In a generator, the heat flow down the temperature gradient

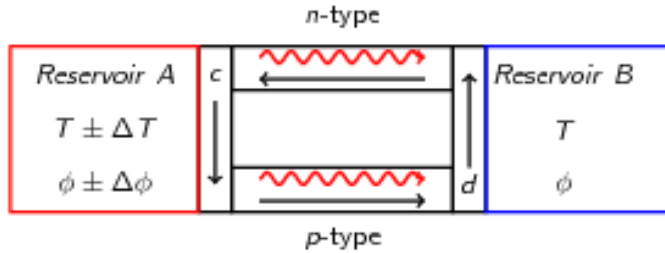


Fig. 1 Schematic representation of a thermoelectric device attached to the reservoirs A and B which are at temperatures $T_A = T$, $T_B = T + \Delta T$ and voltages $\phi_A = \phi$, $\phi_B = \phi \pm \Delta\phi$, respectively. One leg of the device is a p -type and the other an n -type thermoelectric material. The metallic plates c and d ensure a good thermal and electrical contact of all the thermoelectric components with the reservoirs. The straight arrows indicate the circulating charge current. The wiggly arrows indicate the direction of the heat flow.

is accompanied by the circulating electrical current. In a refrigerator, an applied voltage drives the circular current, while the heat flows against the temperature gradient. In both cases, the Carnot cycling relies on the electron fluid and does not require the presence of any mechanical parts.

The applications of the thermoelectric devices are inhibited by their low efficiency and the aim of current research is to produce the materials with better thermoelectric conversion. At high temperatures, the efforts are directed towards the nano-structured semiconductors[2] with reduced heat conductivity. As regards the low-temperature application, the focus is on the materials with strongly correlated electrons, like heavy fermions, valence fluctuators, Kondo insulators and systems with a Mott-Hubbard gap, which can have a large thermopower at low temperatures.

Here, we provide a theoretical description of a simple device built of several conducting planes (the conducting channel) sandwiched between two sets of insulating planes (the barriers). The electron dynamics in all the planes is described by the Falicov-Kimball model and we choose the parameters in such a way that the channel is a delta-doped Mott insulator and the barriers are undoped Mott insulators with a large gap. In such a device, the charge and heat can flow in the direction parallel to the interfaces but not in the perpendicular direction. We assume that the channel and the barriers are made of different ions, so that the phonon scattering on the interfaces is large and the phonon contribution to thermal conductivity is small. Thus, we neglect the phonon contribution to thermal transport and consider only the electron degrees of freedom. By solving the model by the inhomogeneous dynamical

cal mean field theory (DMFT) we find that close to the Mott-Hubbard transition the figure-of-merit becomes very large.

The paper is organized as follows. First, we define the transport coefficients using the phenomenological transport equations for the charge and the internal energy currents parallel to the interfaces. Then, we introduce the microscopic model of the multilayer and derive the appropriate current density operators. We formulate briefly the linear response theory, compute the transport function by the inhomogeneous DMFT and find the solution that satisfies the Poisson equation. Finally, we illustrate the self-consistent solution by showing the numerical results for the transport coefficients and the figure of merit of the device.

2 Phenomenological equation

On a macroscopic level, thermoelectric phenomena are described by irreversible thermodynamics which assumes a local thermodynamic equilibrium within a small volume ΔV around any point \mathbf{x} in the material. The macroscopic current density $\mathbf{J}(\mathbf{x})$ and the internal energy current density $\mathbf{J}_{\mathcal{E}}(\mathbf{x})$ are described by the phenomenological transport equations

$$\mathbf{J}(\mathbf{x}) = -N_{11}(T) \left(\nabla\phi + \frac{T}{e} \nabla \frac{\mu}{T} \right) - N_{12}(T) \frac{\nabla T}{T}, \quad (1)$$

$$\mathbf{J}_{\mathcal{E}}(\mathbf{x}) = -N_{21}(T) \left(\nabla\phi + \frac{T}{e} \nabla \frac{\mu}{T} \right) - N_{22}(T) \frac{\nabla T}{T}.$$

where $\nabla\phi$ is the gradient of the electrical potential, $\nabla\mu$ is the gradient of the chemical potential, ∇T is the temperature gradient, and e is the electrical charge, taken to be negative for electrons and positive for holes. The transport coefficients $N_{ij}(T)$ can either be taken from the experiment or computed for a given microscopic model[1].

The above form of transport equations is convenient for the microscopic calculations, because the coefficients $N_{ij}(T)$ are directly related to various current-current correlation functions. If instead of the internal energy current we use the heat current, $\mathbf{J}_Q = \mathbf{J}_{\mathcal{E}} - \mu\mathbf{J}/e$, the transport coefficients are given by the electrical conductivity, σ , the Seebeck coefficient, α , and the thermal conductivity, κ_e , which are related to the correlation functions in the following way,

$$\sigma(T) = e^2 N_{11}(T), \quad (2)$$

$$\alpha(T) = \left(\frac{k_B}{e} \right) \frac{N_{12}(T)}{T N_{11}(T)}, \quad (3)$$

$$\kappa_e(T) = \left(\frac{k_B}{e} \right)^2 \frac{\sigma(T)}{T} \left[\frac{N_{22}(T)}{N_{11}(T)} - \frac{N_{12}^2(T)}{N_{11}^2(T)} \right]. \quad (4)$$

The efficiency of a particular thermoelectric material depends on the dimensionless figure-of-merit, $ZT = \alpha^2 \sigma T / \kappa$, where $\kappa = \kappa_e + \kappa_{ph}$ is the overall thermal conductivity due to the electronic and the lattice degrees of freedom. The electronic figure-of-merit reads

$$ZT = \frac{[N_{12}(T)]^2}{N_{22}(T)N_{11}(T) - [N_{12}(T)]^2}, \quad (5)$$

and an efficient thermoelectric conversion requires $ZT > 1$.

3 The model Hamiltonian of a correlated multilayer

We consider the multilayer device shown in Fig. 2. There are N insulating planes in the left barrier, N insulating planes in the right barrier and M conducting planes in the central channel, perpendicular to the z -axis. The electron dynamics

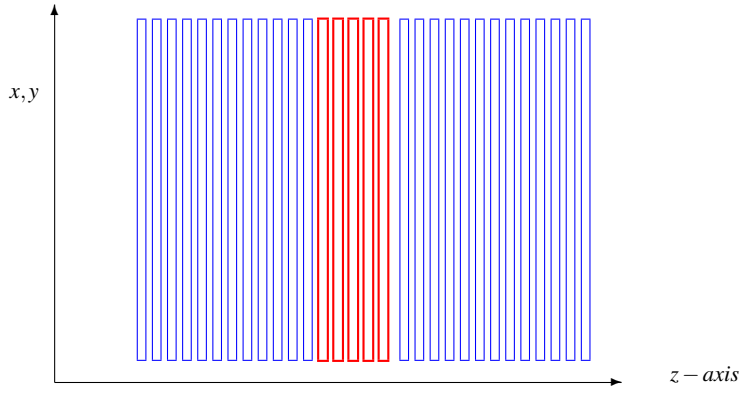


Fig. 2 The cross-section of a multilayer built by N planes in the left and right barriers (represented by thin blue lines) and M planes in the central channel (represented by thick red lines).

is described by a spinless Falicov-Kimball model[3] with large on-site Coulomb interaction. The Hamiltonian is[4, 5]

$$\mathcal{H} = \mathcal{H}_0 + \mathcal{H}_{\text{int}} - \mu \mathcal{N}, \quad (6)$$

where \mathcal{H}_0 is the one-particle Hamiltonian, \mathcal{H}_{int} describes the on-site Falicov-Kimball interaction, and \mathcal{N} is the electron number operator. The one-particle Hamiltonian has several terms, describing the conduction and localized states,

$$\mathcal{H}_0 = \mathcal{H}_T + \mathcal{H}_{\text{offset}} + \mathcal{H}_{\text{charge}} + \mathcal{H}_f. \quad (7)$$

The kinetic-energy term due to the hopping of conduction electrons between the neighboring lattice sites is

$$\mathcal{H}_T = \sum_{\mathbf{r}} h_T^{\mathbf{r}}, \quad (8)$$

where the local kinetic-energy density is written as,

$$h_T^{\mathbf{r}} = -\frac{1}{2} \sum_{\mathbf{d}} (t_{\mathbf{r}+\mathbf{d}}^{\mathbf{r}} c_{\mathbf{r}+\mathbf{d}}^\dagger c_{\mathbf{r}} + t_{\mathbf{r}}^{\mathbf{r}+\mathbf{d}} c_{\mathbf{r}}^\dagger c_{\mathbf{r}+\mathbf{d}}), \quad (9)$$

and the \mathbf{d} summation runs over the nearest neighbors. This form of the local kinetic energy ensures its hermiticity and the symmetry with respect to the left-right hopping (the factor of one-half is due to each term appearing twice when we first sum over \mathbf{d} in $h_T^{\mathbf{r}}$ and then over \mathbf{r} in H_T). The second term of \mathcal{H}_0 describes the difference in the offset of the band-centers in the barrier and the channel planes due to their different chemical composition. Introducing the notation $\mathbf{r} = (\alpha, \mathbf{s})$, where α labels the planes and \mathbf{s} the sites in the α -plane, we write the offset term as,

$$\mathcal{H}_{\text{offset}} = - \sum_{\alpha} \sum_{\mathbf{s} \in \text{plane}} \Delta \mu_{\alpha} c_{\alpha \mathbf{s}}^\dagger c_{\alpha \mathbf{s}}. \quad (10)$$

The mismatch of the electron bands caused by $\mathcal{H}_{\text{offset}}$ gives rise to electronic charge reconstruction and long-range Coulomb interactions. The consistency between the quantum-mechanical description of electrons in the multilayer, defined by the Hamiltonian \mathcal{H} , and the Maxwell equations is ensured by the third term of \mathcal{H}_0 , which reads

$$\mathcal{H}_{\text{charge}} = \sum_{\alpha} V_{\alpha} \sum_{\mathbf{s} \in \text{plane}} c_{\alpha \mathbf{s}}^\dagger c_{\alpha \mathbf{s}}. \quad (11)$$

The local potential V_{α} shifts the electro-chemical potential $\mu \rightarrow \mu - V_{\alpha}$ on each plane and is determined self-consistently from the Poisson equation with the equilibrium charge distribution, ρ_{α} , on each plane[4]. This is obtained by subtracting the contribution of the background ion cores to the net charge on each plane. The number of planes in the barrier has to be large enough that the inhomogeneities due to the channel planes have relaxed back to bulk values when sufficiently far from the interface.

In addition to the conduction states described by the first three terms of \mathcal{H}_0 , we also have on each lattice site a localized level that is either occupied or unoccupied by an f -electron. The distribution of f -electrons is random but annealed. Because the averaging over all possible configurations restores the translational symmetry, we write the Hamiltonian of the localized states as,

$$\mathcal{H}_f = \sum_{\alpha} \sum_{\mathbf{s} \in \text{plane}} (E_{\alpha \mathbf{s}} - \mu_f) f_{\alpha \mathbf{s}}^\dagger f_{\alpha \mathbf{s}} \quad (12)$$

where the chemical potential μ_f determines the average number of f -electrons \mathcal{N}_f . which is taken to be $\mathcal{N}_f = 0.5$ in this work.

The interaction between the itinerant and localized electrons is described by

$$\mathcal{H}_{\text{int}} = \sum_{\alpha} \sum_{\mathbf{s} \in \text{plane}} U_{\alpha} c_{\alpha\mathbf{s}}^{\dagger} c_{\alpha\mathbf{s}} f_{\alpha\mathbf{s}}^{\dagger} f_{\alpha\mathbf{s}}, \quad (13)$$

where U_{α} denotes the short range Coulomb interaction on plane α .

4 The current density operator

We now compute the uniform current density operator that is need for the linear response theory. We introduce the polarization operator, $\hat{\mathbf{P}}_{\rho} = \sum_{\mathbf{r}} \mathbf{r} \hat{\rho}_{\mathbf{r}}$, where $\hat{\rho}_{\mathbf{r}} = c_{\mathbf{r}}^{\dagger} c_{\mathbf{r}}$ is the charge density operator at lattice site \mathbf{r} and define the uniform displacement current as $\hat{\mathbf{j}}_0 = d\hat{\mathbf{P}}_{\rho}/dt$. The equation of motion then yields

$$\hat{\mathbf{j}}_0 = i[\mathcal{H}, \mathbf{P}_{\rho}] = \sum_{\mathbf{r}} \hat{\mathbf{j}}_{\mathbf{r}}^{\text{loc}}, \quad (14)$$

where we introduced the local current density operator

$$\hat{\mathbf{j}}_{\mathbf{r}}^{\text{loc}} = i \mathbf{r} [\mathcal{H}_{\mathbf{r}}, \hat{\rho}_{\mathbf{r}}] = i \mathbf{r} \sum_{\mathbf{r}'} [h_{\mathbf{r}\mathbf{r}}^{\mathbf{r}'}, \hat{\rho}_{\mathbf{r}}]. \quad (15)$$

and the summation over \mathbf{r}' runs over all the lattice sites. The last equation holds because $\hat{\rho}_{\mathbf{r}}$ commutes with all the terms in the Hamiltonian except $\mathcal{H}_{\mathbf{r}}$. To obtain the current parallel to the planes we take \mathbf{r} parallel to the planes and compute

$$\hat{\mathbf{j}}_{\mathbf{r}}^{\text{loc}} = \frac{ie\mathbf{r}}{2} \sum_{\mathbf{r}'} \sum_{\mathbf{d}} [(t_{\mathbf{r}\mathbf{r}+\mathbf{d}}^{\mathbf{r}'} c_{\mathbf{r}}^{\dagger} c_{\mathbf{r}+\mathbf{d}} + t_{\mathbf{r}\mathbf{r}+\mathbf{d}}^{\mathbf{r}'} c_{\mathbf{r}+\mathbf{d}}^{\dagger} c_{\mathbf{r}}), c_{\mathbf{r}}^{\dagger} c_{\mathbf{r}}], \quad (16)$$

which has the only non-vanishing terms for $\mathbf{r}' = \mathbf{r}$ and $\mathbf{r}' = \mathbf{r} - \mathbf{d}$. This gives,

$$\hat{\mathbf{j}}_{\mathbf{r}}^{\text{loc}} = \frac{ie}{2} \sum_{\mathbf{d}} \left\{ t_{\mathbf{r}\mathbf{r}+\mathbf{d}}^{\mathbf{r}} \mathbf{r} [c_{\mathbf{r}}^{\dagger} c_{\mathbf{r}+\mathbf{d}}, c_{\mathbf{r}}^{\dagger} c_{\mathbf{r}}] + t_{\mathbf{r}\mathbf{r}+\mathbf{d}}^{\mathbf{r}} \mathbf{r} [c_{\mathbf{r}+\mathbf{d}}^{\dagger} c_{\mathbf{r}}, c_{\mathbf{r}}^{\dagger} c_{\mathbf{r}}] \right\} \quad (17)$$

$$\begin{aligned} &+ \frac{i}{2} \sum_{\mathbf{d}} \left\{ t_{\mathbf{r}\mathbf{r}+\mathbf{d}}^{\mathbf{r}} (\mathbf{r} + \mathbf{d}) [c_{\mathbf{r}}^{\dagger} c_{\mathbf{r}+\mathbf{d}}, c_{\mathbf{r}+\mathbf{d}}^{\dagger} c_{\mathbf{r}+\mathbf{d}}] + t_{\mathbf{r}\mathbf{r}+\mathbf{d}}^{\mathbf{r}} (\mathbf{r} + \mathbf{d}) [c_{\mathbf{r}+\mathbf{d}}^{\dagger} c_{\mathbf{r}}, c_{\mathbf{r}+\mathbf{d}}^{\dagger} c_{\mathbf{r}+\mathbf{d}}] \right\}, \\ &= \frac{ie}{2} \sum_{\mathbf{d}} \mathbf{d} (t_{\mathbf{r}\mathbf{r}+\mathbf{d}}^{\mathbf{r}} c_{\mathbf{r}}^{\dagger} c_{\mathbf{r}+\mathbf{d}} - t_{\mathbf{r}\mathbf{r}+\mathbf{d}}^{\mathbf{r}} c_{\mathbf{r}+\mathbf{d}}^{\dagger} c_{\mathbf{r}}) \end{aligned} \quad (18)$$

and the uniform current is obtained by summing $\hat{\mathbf{j}}_{\mathbf{r}}^{\text{loc}}$ over all the sites,

$$\hat{\mathbf{j}}_0 = \sum_{\alpha} \sum_{\mathbf{s}} \hat{\mathbf{j}}_{\mathbf{s}\alpha}, \quad (19)$$

where α is the plane index and \mathbf{s} is the lattice vector within the plane, i.e., $\mathbf{r} = (\alpha, \mathbf{s})$. Introducing the two-dimensional Fourier transform $c_{\mathbf{q}\alpha} = \sum_{\mathbf{s}} e^{i\mathbf{q}\cdot\mathbf{s}} c_{\mathbf{s}\alpha}/L$, where \mathbf{q} is

the 2-D reciprocal lattice vector for plane α , we obtain the Fourier transform of the local current density operator,

$$\hat{\mathbf{j}}_{\mathbf{p}\alpha} = \sum_{\mathbf{q}} \mathbf{v}_{\mathbf{q}} c_{\mathbf{p}+\mathbf{q},\alpha}^\dagger c_{\mathbf{q}\alpha} . \quad (20)$$

Here, we introduced the in-plane velocity $\mathbf{v}_{\mathbf{q}} = \nabla_{\mathbf{q}} \varepsilon_{\mathbf{q}}$ and the unperturbed dispersion $\varepsilon_{\mathbf{q}}$. In the long-wavelength limit, the summing over all the planes yields the total current,

$$\hat{\mathbf{j}}_0 = \lim_{\mathbf{p} \rightarrow 0} \sum_{\alpha} \hat{\mathbf{j}}_{\mathbf{p}\alpha} = \sum_{\mathbf{q}\alpha} \mathbf{v}_{\mathbf{q}} c_{\mathbf{q}\alpha}^\dagger c_{\mathbf{q}\alpha} . \quad (21)$$

The calculation of the local energy current proceeds along exactly the same lines but requires more complicated commutators since now the potential energy terms do not commute with the energy polarization operator. Then a similar calculation provides for the energy current that is simply related to $\hat{\mathbf{j}}_{s\alpha}$. We do not show an explicit expression for the energy or heat current operator here, because we can evaluate all relevant expectation values by employing the Jonson-Mahan theorem, as described below.

5 The linear response theory

The transport coefficients of a multilayer described by our model are obtained by computing the quantum-mechanical averages,

$$\mathbf{J}^i(\mathbf{x}) = \text{Tr}\{\rho_\phi \hat{\mathbf{j}}_0^i(\mathbf{x})\}, \quad (22)$$

where $\hat{\mathbf{j}}_0^i$ is the current density operator along the i -axis, ρ_ϕ is the density matrix of the particles moving in an external potential $\phi(\mathbf{x}, t)$ which grows continuously from $t = -\infty$ up to $t = 0$, with the characteristic switching-on time $\tau_\phi = 1/\omega$. The vector \mathbf{x} denotes the center of the small but macroscopic region which is considered to be in thermal equilibrium. The electrical field $\mathbf{E} = -\nabla\phi$ is applied parallel to the multilayer planes and varies in space on the scale $\lambda_{\mathbf{q}} \simeq 1/|\mathbf{q}|$, such that for $\mathbf{q} \rightarrow 0$ the perturbation is uniform over the sample. The current response for $t \geq 0$ is obtained from the gradient expansion of the density matrix [1] which gives

$$\mathbf{J}^i(\mathbf{x}) = e^{\omega t} \sum_j \int d\mathbf{x}' \mathbf{E}^j(\mathbf{x}') \int_0^\infty dt' e^{-\omega t'} \int_0^\beta d\beta' \langle \hat{\mathbf{j}}^j(\mathbf{x}', -t' - i\beta') \hat{\mathbf{j}}^i(\mathbf{x}) \rangle_0 , \quad (23)$$

where $\langle \dots \rangle_0$ denotes the thermodynamic average with respect to the unperturbed density matrix $\hat{\rho}_0$ and index j labels the coordinate axes. The static conductivity is obtained by Fourier transforming Eq. (23) and taking the $\mathbf{q} \rightarrow 0$ limit before the $\omega \rightarrow 0$ limit. This gives

$$\sigma^{ij} = \lim_{\omega \rightarrow 0} \sigma^{ij}(\omega) = V \lim_{\omega \rightarrow 0} \int_0^\infty dt' e^{-\omega t'} \int_0^\beta d\beta' \langle \hat{\mathbf{j}}_0^j(-t' - i\beta') \hat{\mathbf{j}}_0^i \rangle_0, \quad (24)$$

where $\hat{\mathbf{j}}_0^j$ is the uniform current density operator derived in the previous section. Using the basis which diagonalizes the Hamiltonian, we can write Eq. (24) as

$$\sigma^{ij} = \lim_{\omega \rightarrow 0} \sigma(\omega) = V \pi\beta \sum_{mn} e^{\beta(\Omega - E_n)} \langle n | \hat{\mathbf{j}}_0^j | m \rangle \langle m | \hat{\mathbf{j}}_0^i | n \rangle \delta(E_n - E_m). \quad (25)$$

This is equivalent to Kubo formula,

$$\sigma^{ij} = - \lim_{\omega \rightarrow 0} \frac{\text{Im } \mathcal{N}^{ij}(\omega)}{\omega}, \quad (26)$$

where $\mathcal{N}^{ij}(\omega)$ is the Fourier transform of the retarded correlation function,

$$\mathcal{N}^{ij}(t - t') = -i \Theta(t - t') \langle \hat{\mathbf{j}}_0^j(t') \hat{\mathbf{j}}_0^i(t) - \hat{\mathbf{j}}_0^i(t) \hat{\mathbf{j}}_0^j(t') \rangle_0. \quad (27)$$

The equivalence of expression (26) to (25) is seen at once by using the basis which diagonalizes \mathcal{H} and writing the Fourier transform of $\mathcal{N}^{ij}(t - t')$ as,

$$\mathcal{N}^{ij}(\omega) = e^{\beta\Omega} \sum_{mn} \langle n | \hat{\mathbf{j}}_0^j | m \rangle \langle m | \hat{\mathbf{j}}_0^i | n \rangle \frac{e^{-\beta E_n} - e^{-\beta E_m}}{\omega + E_n - E_m + i\delta}. \quad (28)$$

The imaginary part is then

$$\text{Im } \mathcal{N}^{ij}(\omega) = (1 - e^{-\beta\omega}) \sum_{mn} e^{\beta(\Omega - E_n)} \langle n | \hat{\mathbf{j}}_0^j | m \rangle \langle m | \hat{\mathbf{j}}_0^i | n \rangle \delta(\omega + E_n - E_m) \quad (29)$$

and dividing by ω and taking the $\omega \rightarrow 0$ limit yields the same result as given by the Luttinger formula in Eq. (25). The advantage of the Kubo formula is that the retarded Green's function can be obtained by analytically continuing the time-ordered one from the imaginary to the real frequency axis[7].

6 The transport function

To find the transport coefficients we assume the equivalence of the x and y coordinate axes, drop the axis label, and consider the imaginary-time current-current correlation function which is periodic on the interval $\tau \in (0, \beta)$. Its Fourier transform is defined for Bosonic Matsubara frequencies, $i\nu_l = 2\pi n/\beta$,

$$\begin{aligned} \mathcal{N}(i\nu_l) &= \int_0^\beta d\tau e^{i\nu_l \tau} \langle \mathcal{T}_\tau \hat{\mathbf{j}}_0(\tau) \hat{\mathbf{j}}_0(0) \rangle \\ &= \sum_{\alpha\beta} \int_0^\beta d\tau e^{i\nu_l \tau} \langle \mathcal{T}_\tau \hat{\mathbf{j}}_{0\alpha}(\tau) \hat{\mathbf{j}}_{0\beta}(0) \rangle \end{aligned}$$

$$= \sum_{\alpha\beta} \mathcal{N}_{\alpha\beta}(i\nu_l). \quad (30)$$

Using the definition of the uniform current density on plane α we write the non-local correlation function as,

$$\mathcal{N}_{\alpha\beta}(i\nu_l) = e^2 \sum_{\mathbf{q}} \sum_{\mathbf{p}} \frac{(\mathbf{v}_{\mathbf{q}})^2}{2} \int_0^\beta d\tau e^{i\nu_l \tau} \langle \mathcal{T}_\tau c_{\mathbf{q}\alpha}^\dagger(\tau) c_{\mathbf{q}\alpha}(\tau) c_{\mathbf{p}\beta}^\dagger c_{\mathbf{p}\beta} \rangle, \quad (31)$$

and evaluate it by the Wick's theorem, neglecting the vertex corrections. Because of translational invariance within the planes, the $2-D$ momentum \mathbf{q} is a good quantum number, and the single particle Green's function can be written in the mixed (α, \mathbf{q}) representation as, $G_{\alpha\beta}^{\mathbf{q}}(\tau) = -\langle \mathcal{T}_\tau c_{\mathbf{q}\alpha}^\dagger(\tau) c_{\mathbf{q}\beta} \rangle$. Taking into account that the Green's function is even, while the velocity is odd in bfq , we write

$$\mathcal{N}_{\alpha\beta}(i\nu_l) = -e^2 \sum_{\mathbf{q}} \frac{(\mathbf{v}_{\mathbf{q}})^2}{2} \int_0^\beta d\tau e^{i\nu_l \tau} G_{\alpha\beta}^{\mathbf{q}}(\tau) G_{\beta\alpha}^{\mathbf{q}}(-\tau). \quad (32)$$

The above derivation is exact in infinite dimensions, where the vertex corrections vanish and holds in two dimensions when we use the approximation of a local self-energy. The τ -integration is performed by substituting the Fourier transform

$$G_{\alpha\beta}^{\mathbf{q}}(\tau) = T \sum_n e^{-i\omega_n \tau} G_{\alpha\beta}^{\mathbf{q}}(i\omega_n)$$

which gives

$$\mathcal{N}_{\alpha\beta}(i\nu_l) = -e^2 \pi T \sum_{\mathbf{q}} \frac{(\mathbf{v}_{\mathbf{q}})^2}{2} \sum_n G_{\alpha\beta}^{\mathbf{q}}(i\omega_n) G_{\beta\alpha}^{\mathbf{q}}(i\omega_n + i\nu_l). \quad (33)$$

The analytic continuation of $\mathcal{N}_{\alpha\beta}(i\nu_l)$ from the imaginary to real axis is now straightforward[7]. We first write the summation over Matsubara frequencies as an integral over the contour C which has contributions at the poles of the Fermi function $f(\omega) = 1/[1 + \exp(\beta\omega)]$ which lie at the Fermionic Matsubara frequencies. The contours are then deformed to lines parallel to the real axis, with the Green's functions evaluated with either retarded (R) or advanced (A) functions. The result is

$$\begin{aligned} \mathcal{N}_{\alpha\beta}(i\nu_l) &= -\frac{e^2}{2i} \int_{-\infty}^{\infty} d\omega f(\omega) \sum_{\mathbf{q}} \frac{(\mathbf{v}_{\mathbf{q}})^2}{2} [G_{\alpha\beta}^{\mathbf{q}R}(\omega) - G_{\alpha\beta}^{\mathbf{q}A}(\omega)] G_{\alpha\beta}^{\mathbf{q}R}(\omega + i\nu_l) \\ &\quad - \frac{e^2}{2i} \int_{-\infty}^{\infty} d\omega f(\omega) \sum_{\mathbf{q}} \frac{(\mathbf{v}_{\mathbf{q}})^2}{2} [G_{\alpha\beta}^{\mathbf{q}R}(\omega) - G_{\alpha\beta}^{\mathbf{q}A}(\omega)] G_{\alpha\beta}^{\mathbf{q}A}(\omega - i\nu_l), \quad (34) \end{aligned}$$

where (R) and (A) label the retarded and advanced Green's functions. Since the retarded and advanced Green's function have well defined analytic properties in the upper and lower part of the complex ω -plane, respectively, they can be analytically continued just by replacing $\omega \pm i\nu_l \rightarrow \omega \pm (\nu + i\delta)$. This gives

$$\begin{aligned} \mathcal{N}_{\alpha\beta}(\nu) &= -\frac{e^2}{2i} \sum_{\mathbf{q}} \frac{(\mathbf{v}_{\mathbf{q}})^2}{2} \int_{-\infty}^{\infty} d\omega f(\omega) [G_{\alpha\beta}^{\mathbf{qR}}(\omega) - G_{\alpha\beta}^{\mathbf{qA}}(\omega)] G_{\alpha\beta}^{\mathbf{qR}}(\omega + \nu) \\ &\quad - \frac{e^2}{2i} \sum_{\mathbf{q}} \frac{(\mathbf{v}_{\mathbf{q}})^2}{2} \int_{-\infty}^{\infty} d\omega f(\omega + \nu) [G_{\alpha\beta}^{\mathbf{qR}}(\omega + \nu) - G_{\alpha\beta}^{\mathbf{qA}}(\omega + \nu)] G_{\alpha\beta}^{\mathbf{qA}}(\omega), \end{aligned} \quad (35)$$

where the integration variable in the second integral has been shifted by $\omega \rightarrow \omega + \nu$. Taking the imaginary part and dividing by ν yields

$$\begin{aligned} \lim_{\nu \rightarrow 0} \frac{\text{Im } \mathcal{N}_{\alpha\beta}(\nu)}{\nu} &= e^2 \sum_{\mathbf{q}} \frac{(\mathbf{v}_{\mathbf{q}})^2}{2\nu} \int_{-\infty}^{\infty} d\omega \quad \lim_{\nu \rightarrow 0} \left[f(\omega) \text{Im } G_{\alpha\beta}^{\mathbf{qR}}(\omega) \text{Im } G_{\alpha\beta}^{\mathbf{qR}}(\omega + \nu) \right. \\ &\quad \left. - f(\omega + \nu) \text{Im } G_{\alpha\beta}^{\mathbf{qR}}(\omega + \nu) \text{Im } G_{\alpha\beta}^{\mathbf{qR}}(\omega) \right]. \end{aligned} \quad (36)$$

Thus, the static conductivity matrix can be written as,

$$\sigma_{\alpha\beta} = -\lim_{\nu \rightarrow 0} \frac{\text{Im } \mathcal{N}_{\alpha\beta}(\nu)}{\nu} = e^2 \sum_{\mathbf{q}} \frac{(\mathbf{v}_{\mathbf{q}})^2}{2} \int_{-\infty}^{\infty} d\omega \left(-\frac{\partial f(\omega)}{\partial \omega} \right) [\text{Im } G_{\alpha\beta}^{\mathbf{qR}}(\omega)]^2. \quad (37)$$

The retarded single-particle Green's function depends on the planar momentum through the plane-wave energy $\epsilon_{\mathbf{q}}$, so that the \mathbf{q} -summation can be performed by introducing the transport density of states (DOS)

$$\rho_{tr}^{2D}(\epsilon) = \sum_{\mathbf{q}} \mathbf{v}_{\mathbf{q}}^2 \delta(\epsilon - \epsilon_{\mathbf{q}}). \quad (38)$$

This is easily found for the square lattice by solving the differential equation

$$\frac{d\rho_{tr}^{2D}(\epsilon)}{d\epsilon} = -\frac{\epsilon}{4} \rho_{2D}(\epsilon),$$

and using the boundary condition $\rho_{tr}^{2D}(-D) = 0$, where $-D$ is the bottom of the conduction band, and $\rho_{2D}(\epsilon)$ is the density of states for nearest-neighbor hopping on a square lattice. The result for ρ_{tr}^{2D} is plotted in Fig.3, which shows that even though ρ^{2D} is logarithmically singular, the transport DOS is a smooth function for all the band energies.

The static conductivity for transport parallel to the multilayer planes can be written as a sum

$$\sigma(T) = \sum_{\alpha} \sigma_{\alpha}, \quad (39)$$

where σ_{α} is the planar conductivity

$$\sigma_{\alpha} = e^2 \int_{-\infty}^{\infty} d\omega \left(-\frac{\partial f(\omega)}{\partial \omega} \right) \Lambda_{tr}^{\alpha}(\omega), \quad (40)$$

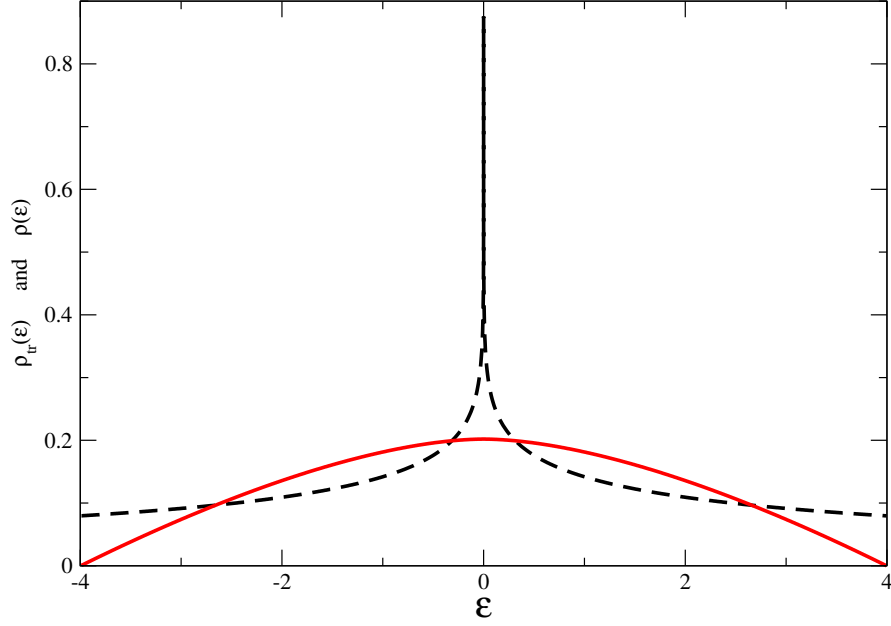


Fig. 3 Two dimensional density of states (dashed line) and the transport density of states (full line) for the square lattice are plotted versus energy.

and we introduced the transport function for plane α ,

$$\Lambda_{tr}^{\alpha}(\omega) = \sum_{\beta} \int d\epsilon \rho_{tr}^{2D}(\epsilon) [\text{Im} G_{\alpha\beta}(\epsilon, \omega)]^2. \quad (41)$$

Since the Falicov-Kimball model satisfies the Jonson-Mahan theorem [6, 5], the other transport integrals are obtained by integrating the same transport function,

$$N_{mn}(T) = \sum_{\alpha} \int_{-\infty}^{\infty} d\omega \left(-\frac{\partial f(\omega)}{\partial \omega} \right) \omega^{m+n-2} \Lambda_{tr}^{\alpha}(\omega). \quad (42)$$

7 The Green's functions of a multilayer

We now calculate the transport function for the Hamiltonian in equation (6). From the definition of the Green's function, $(z - H)G = 1$, we obtain the secular equation in real space,

$$zG_{\alpha\beta}(\mathbf{p} - \mathbf{r}) - \sum_{\gamma\mathbf{s}} H_{\alpha\gamma}(\mathbf{p} - \mathbf{s})G_{\gamma\beta}(\mathbf{s} - \mathbf{j}) = \delta_{\alpha\beta} \delta(\mathbf{r} - \mathbf{p}), \quad (43)$$

where $\mathbf{p}, \mathbf{s}, \mathbf{r}$ are the 2-D lattice vectors and we used the translational invariance in the (x, y) direction. Restricting the hopping matrix elements to nearest neighbors, we write the non-interacting ($U = 0$) Green's function as

$$\begin{aligned} zG_{\alpha\beta}^0(\mathbf{p}-\mathbf{r}) &= \sum_{\mathbf{s}} H_{\alpha\alpha}(\mathbf{p}-\mathbf{s})G_{\alpha\beta}^0(\mathbf{s}-\mathbf{j}) \\ &\quad - \sum_{\mathbf{s}} \left[H_{\alpha\alpha-1}(\mathbf{p}-\mathbf{s})G_{\alpha-1\beta}^0(\mathbf{s}-\mathbf{j}) + H_{\alpha\alpha+1}(\mathbf{p}-\mathbf{s})G_{\alpha+1\beta}^0(\mathbf{s}-\mathbf{j}) \right] \\ &= \delta_{\alpha\beta} \delta(\mathbf{r}-\mathbf{p}) . \end{aligned} \quad (44)$$

Substituting the in-plane Fourier transform, $G_{\alpha\beta}^0(i\mathbf{q}, z) = \sum_{\mathbf{r}} G_{\alpha\beta}(\mathbf{r}, z) \exp\{\mathbf{q} \cdot \mathbf{r}\}$, we find the \mathbf{q} -component of the non-interacting Green's function,

$$\sum_{\gamma} \left[[z + \mu - \varepsilon_{\alpha}^{\parallel}(\mathbf{q})] \delta_{\alpha\gamma} + t_{\alpha}^{\alpha-1} \delta_{\alpha-1, \gamma} + t_{\alpha}^{\alpha+1} \delta_{\alpha+1, \gamma} \right] G_{\gamma\beta}^0(\mathbf{q}, z) = \delta_{\alpha\beta} , \quad (45)$$

where we introduced the mixed representation and used the fact that the matrix element for the hopping to the neighboring planes is the same for each point on the plane. By definition, the inverse matrix of $G_{\alpha\gamma}^0$ is given by the square bracket in Eq. (45). The renormalized Green's function follows from the Dyson equation, which reads in the mixed representation

$$G_{\alpha\beta}(\mathbf{q}, z) = G_{\alpha\beta}^0(\mathbf{q}, z) + \sum_{\gamma} G_{\alpha\gamma}^0(\mathbf{q}, z) \Sigma_{\gamma\gamma}(z) G_{\gamma\beta}(\mathbf{q}, z) . \quad (46)$$

The self energy is different on each plane but, in the spirit of the DMFT approximation, it is assumed to be diagonal in planar indices and independent of the two-dimensional momentum. The matrix elements $G_{\alpha\beta}(\mathbf{q}, z)$ satisfy the EOM which is obtained by multiplying Eq. (46) from the left by the inverse matrix of $G_{\alpha\beta}^0$ which yields

$$\left[z + \mu - \Sigma_{\alpha}(z) - \varepsilon_{\alpha}^{\parallel}(\mathbf{q}) \right] G_{\alpha\beta}(\mathbf{q}, z) + t_{\alpha}^{\alpha-1} G_{\alpha-1\beta}(\mathbf{q}, z) + t_{\alpha}^{\alpha+1} G_{\alpha+1\beta}(\mathbf{q}, z) = \delta_{\alpha\beta} \quad (47)$$

where $\varepsilon_{\alpha\mathbf{q}}^{\parallel} = \sum_{\mathbf{r}} t_{\alpha}^{\alpha}(\mathbf{r}) \exp\{i\mathbf{q} \cdot \mathbf{r}\}$ is the dispersion for plane α . The diagonal Green's function can be written as

$$G_{\alpha\alpha}(\mathbf{q}, z) = \frac{1}{L_{\alpha}(\mathbf{q}, z) + R_{\alpha}(\mathbf{q}, z) - \left[z + \mu - \Sigma_{\alpha}(z) - \varepsilon_{\alpha}^{\parallel}(\mathbf{q}) \right]} . \quad (48)$$

where we introduced two auxiliary functions

$$L_{\alpha-n}(\mathbf{q}, z) = -t_{\alpha-n}^{\alpha-n+1} \frac{G_{\alpha-n+1, \alpha}(\mathbf{q}, z)}{G_{\alpha-n, \alpha}(\mathbf{q}, z)} \quad (49)$$

and

$$R_{\alpha+n}(\mathbf{q}, z) = -t_{\alpha+n}^{\alpha+n-1} \frac{G_{\alpha+n-1, \alpha}(\mathbf{q}, z)}{G_{\alpha+n, \alpha}(\mathbf{q}, z)}. \quad (50)$$

The index α runs from the first ($\alpha = 0$) to the last ($\alpha = N$) plane of the multilayer and n in Eqs. (49) and (50) satisfies $0 \leq \alpha - n \leq N$ and $0 \leq \alpha + n \leq N$, respectively. Functions $L_{\alpha-n}$ and $R_{\alpha-n}$ satisfy the recursion relations which follow from the EOM for the off-diagonal matrix elements $G_{\alpha\beta}$. Setting in Eq. (47) $\beta \rightarrow \alpha$ and $\alpha \rightarrow \alpha - n$ and using Eq. (49) gives

$$L_{\alpha-n}(\mathbf{q}, z) = z + \mu - \Sigma_{\alpha-n}(z) - \varepsilon_{\alpha-n}^{\parallel}(\mathbf{q}) - \frac{t_{\alpha-n}^{\alpha-n-1} t_{\alpha-n-1}^{\alpha-n}}{L_{\alpha-n-1}(\mathbf{q}, z)}, \quad (51)$$

while setting $\beta \rightarrow \alpha$ and $\alpha \rightarrow \alpha + n$ and using (50) gives,

$$R_{\alpha+n}(\mathbf{q}, z) = z + \mu - \Sigma_{\alpha+n}(z) - \varepsilon_{\alpha+n}^{\parallel}(\mathbf{q}) - \frac{t_{\alpha+n}^{\alpha+n+1} t_{\alpha+n+1}^{\alpha+n}}{R_{\alpha+n+1}(\mathbf{q}, z)}. \quad (52)$$

We now assume that far enough from the central planes the Green's functions become independent of the plane index, so that $L_{\alpha-n}(\mathbf{q}, z) \simeq L_0(\mathbf{q}, z)$ and $R_{\alpha+n}(\mathbf{q}, z) \simeq R_N(\mathbf{q}, z)$. In this asymptotic regime, Eqs. (51) and (52) become quadratic equations for L_0 and R_N with the solutions

$$L_0(\mathbf{q}, z) = \frac{z + \mu - \Sigma_0(z) - \varepsilon_0^{\parallel}(\mathbf{q})}{2} \pm \sqrt{[z + \mu - \Sigma_0(z) - \varepsilon_0^{\parallel}(\mathbf{q})]^2 - 4t_0^2}, \quad (53)$$

and

$$R_N(\mathbf{q}, z) = \frac{z + \mu - \Sigma_N(z) - \varepsilon_N^{\parallel}(\mathbf{q})}{2} \pm \sqrt{[z + \mu - \Sigma_N(z) - \varepsilon_N^{\parallel}(\mathbf{q})]^2 - 4t_N^2}, \quad (54)$$

If we know $\Sigma_{\alpha}(z)$ on each plane, we can generate all other auxiliary functions L_1, L_2, \dots, L_N and $R_{N-1}, R_{N-2}, \dots, R_0$ from L_0 and R_N . For example, L_1 and R_{N-1} are obtained by setting $n = \alpha - 1$ in Eq. (51) and $n = N - \alpha - 1$ in Eq. (52). Knowing L_{α} , R_{α} , and $\Sigma_{\alpha}(z)$ for each plane we get the planar Green's function $G_{\alpha\alpha}(z)$ from Eq. (48).

8 The inhomogeneous DMFT solution

We now consider the DMFT solution for the multilayer described by the Falicov-Kimball model with N insulating (barrier) planes on the left and on the right, and M metallic (channel) planes in-between. The channel planes are made metallic by delta-doping a Mott insulator, i.e., the channel planes are close to the insulating phase. The first plane in the multilayer is indexed by $\alpha = 0$ and the last one by $\alpha = 2N + M$.

The single particle Green's function which determines the transport function is calculated by the inhomogeneous dynamical mean-field (DMFT) theory[8, 4, 5]. The hopping is taken as $t_\alpha^\alpha = t_\alpha^{\alpha\pm 1} = t$, such the dispersion and velocity are the same on all planes and given by $\varepsilon(\mathbf{q}) = -t [\cos(q_x a_x) + \cos(q_y a_y)]$ and $v(\mathbf{q}) = \nabla \varepsilon(\mathbf{q})$, respectively. Functions $G_{\alpha\alpha}(\mathbf{q}, z)$, $L_{\alpha-n}(\mathbf{q}, z)$, and $R_{\alpha-n}(\mathbf{q}, z)$ depend on \mathbf{q} only via $\varepsilon(\mathbf{q})$ which allows us to write the local Green's function for each plane as an integral over a 2-dimensional density of states,

$$G_\alpha(z) = \int d\varepsilon \rho_{2D}(\varepsilon) \frac{1}{L_\alpha(\varepsilon, z) + R_\alpha(\varepsilon, z) - [z + \mu - \Sigma_\alpha(z) - \varepsilon]} . \quad (55)$$

where

$$\rho_{2D}(\varepsilon) = \sum_{\mathbf{q}} \delta(\varepsilon - \varepsilon(\mathbf{q})) . \quad (56)$$

For a simple square lattice, $\rho_{2D}(\varepsilon)$ is logarithmically singular.

The DMFT solution for the $2N + M$ planes is obtained by identifying $G_\alpha(z)$ in Eq. (55) with the Green's function of a single-site Falicov-Kimball model and defining the effective medium as,

$$[G_{0\alpha}(z)]^{-1} = [G_\alpha(z)]^{-1} + \Sigma_\alpha(z) . \quad (57)$$

The above equations define the mapping between the lattice problem and $2N + M$ inter-connected single-site Falicov-Kimball problems, where the self-energy $\Sigma_\alpha(z)$ describes the renormalization of the effective conduction electron at site α by the Falicov-Kimball interaction. The mapping is exact in infinite dimensions, where the self-energy functionals of the lattice and the single-site model are defined by identical momentum-independent skeleton diagrams. In a multilayer, the mapping holds only if we neglect the momentum-dependence of all the self-energy diagrams. In that case we can use the well-known solution of the single-site Falicov-Kimball model with \mathcal{N}_f localized f -electrons per site and write

$$G_\alpha(z) = (1 - \mathcal{N}_f)G_{0\alpha}(z) + \frac{\mathcal{N}_f}{[G_{0\alpha}(z)]^{-1} - U_\alpha} . \quad (58)$$

If we use $G_{0\alpha}(z)$ given by Eq. (57) and $G_\alpha(z)$ given by Eq. (58) to recalculate the self energy,

$$\Sigma_\alpha(z) = [G_{0\alpha}(z)]^{-1} - [G_\alpha(z)]^{-1} , \quad (59)$$

we can find the DMFT solution of the lattice problem by iterating Eqs. (55 – 59) to the fixed point. From the stable solution for $\Sigma_\alpha(z)$ we can calculate L_α and R_α and find $G_\alpha(\varepsilon, z)$ for each plane and obtain the transport function of a given plane from Eq. (41). Finally, Eq. (40) yields the conductivity due to all the planes.

9 The numerical results

The numerical results are obtained for a multilayer with 31 planes in the left and the right barrier and 5 planes in the central channel. The Coulomb interaction is set to $U_B = U_C = 8$ and the concentration of the scattering sites (the number of f -electrons) is set to $\mathcal{N}_f = 1/2$. The calculations are performed for several offsets of the band-centers in the barriers and the channel. In all the cases the barriers are Mott insulators and the offset in the central channel makes it a bad metal close to the metal-insulator transition. The bulk transport coefficients obtained for the same band-offsets as in the central channel are computed, for comparison, as well. The energy and temperature are measured in units of the hopping.

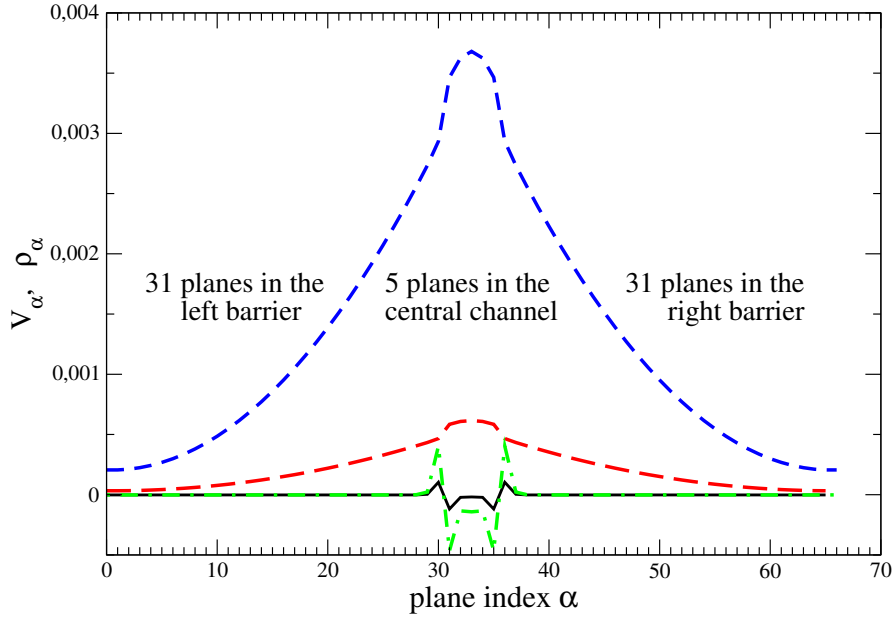


Fig. 4 (*Color online*) The reconstructed charges and the planar potentials plotted versus the plane index α . The first barrier plane is at $\alpha = 0$, the first channel plane is at $\alpha = 31$, the last channel plane is at $\alpha = 36$, and the last barrier plane is at $\alpha = 66$. The results for $\Delta\mu_B = 0.75$ and two values of $\Delta\mu_C$ are shown. The full and the dashed-dotted lines show the local charge, while the dashed and the long-dashed lines show the local potential obtained for $\Delta\mu_C = 0.85$ and $\Delta\mu_C = 0.95$, respectively.

The electronic charge reconstruction and the planar potentials, obtained for $N = 41$ and $M = 5$, are shown in Fig. 4 as a function of the planar index α . We show the results for the offsets chosen to be $\Delta\mu_B = 0.75$ in the barriers and two values of $\Delta\mu_C$ in the channel planes. A nonzero $\Delta\mu_B$ can be thought of as a gate voltage

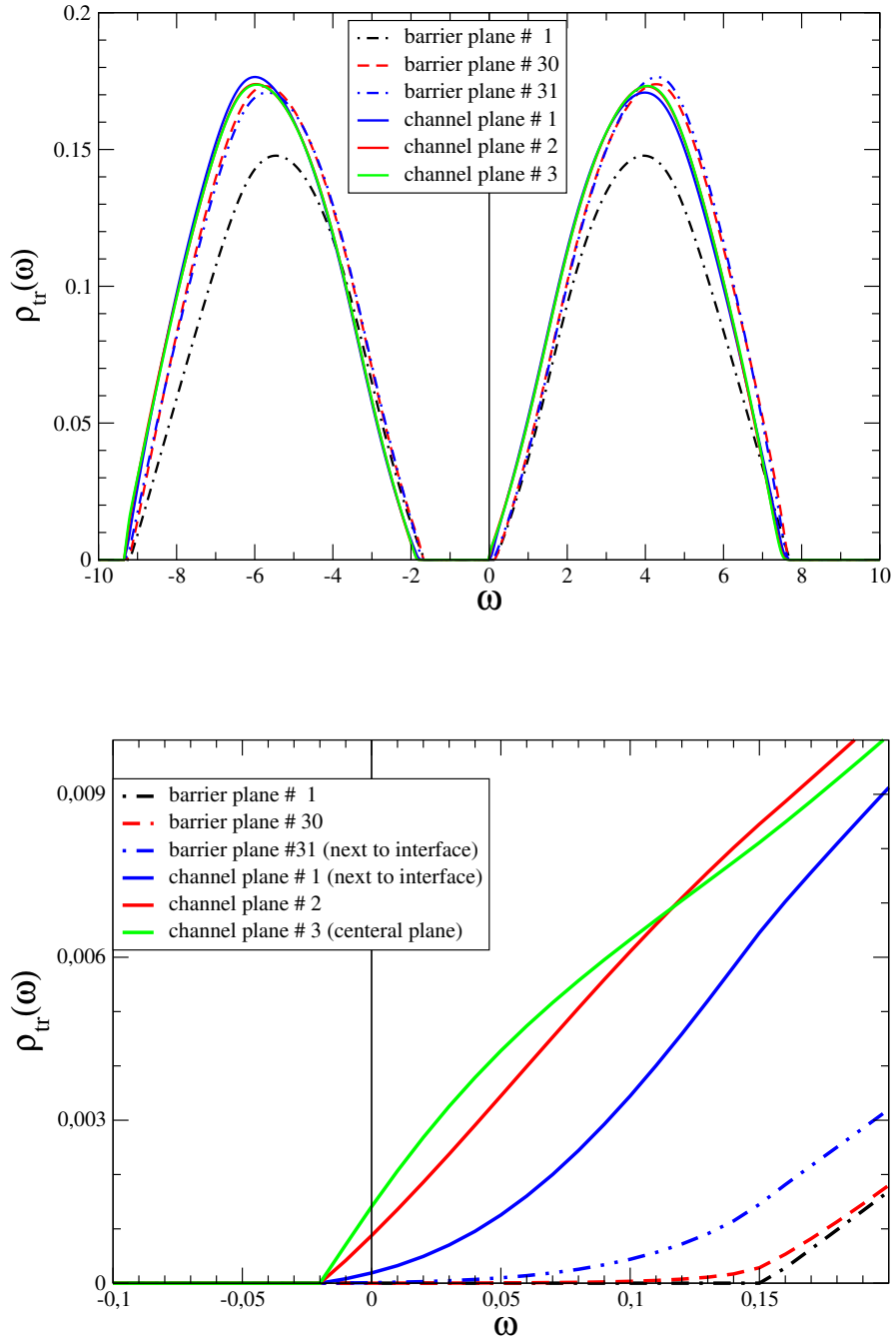


Fig. 5 (Color online) The upper panel shows the transport density of states ρ_{tr}^{α} plotted versus frequency ω for various planes, as indicated in the figure. The lower panel shows the low-frequency part of ρ_{tr}^{α} . The Coulomb interaction in the barriers and channel planes is $U = 8$. The offsets are $\Delta\mu_B = 0.75$ in the barriers and $\Delta\mu_C = 0.75$ in the channel planes. The first barrier plane is at $\alpha = 0$, the last plane in the left barrier is at $\alpha = 31$. There are 5 channel planes.

applied to the entire device, while $\Delta\mu_B \neq \Delta\mu_C$ yields a chemical potential mismatch between the Mott insulator and the conducting channel. The deviation of ρ_α from the bulk values depends on that mismatch, as indicated in Fig. 4, which shows that ρ_α and V_α increase rapidly with the difference between $\Delta\mu_B$ and $\Delta\mu_C$. A homogeneous bulk material with the offset $\Delta\mu_C \leq 0.85$, is a half-filled Mott insulator. The spectral function of the bulk material obtained for $\Delta\mu_C = 0.95$ is also gapped but the chemical potential is in the upper Hubbard band, close to the gap-edge, which defines a 'delta-doped' Mott insulator. The potential and the charge satisfy the Poisson equation: the charge deviates most strongly from the bulk values close to the interface, where the curvature of the local potential changes sign. The potential has the maximum in the center of the barrier and decays very slowly to the bulk values ($V_{bulk} = 0$) as we go away from the interface. The self-consistency of the solution requires a large number of the planes in the barrier, which makes the calculations numerically demanding. (For details regarding the effect of the screening length on the charge reconstruction see Ref. [4].)

The overall features of the transport DOS of the multilayer, calculated for the offsets $\Delta\mu_B = 0.75$ and $\Delta\mu_C = 0.90$ are shown in the Figs. 5, where we plot ρ_{ir}^α for several multilayer planes, as indicated in the figure. The Coulomb interaction is large enough to open the gap in $\rho_{ir}^\alpha(\omega)$ in the barriers and channel planes. A bulk material with the same band-center offset as the barrier planes is a Mott insulator. The bulk material with the offset as the channel planes is a 'delta doped' Mott insulator. Such a 'bad metal' has the chemical potential in the upper Hubbard band, where $\rho_{ir}^{bulk}(\omega) \neq 0$ and the slope of $\rho_{ir}^{bulk}(\omega)$ is very steep. These features are preserved in the multilayer, except for the distortion of ρ_{ir}^α close to the interface. For a constant concentration of f -electrons, the transport density of states is independent of temperature. The low-energy part of ρ_{ir}^α is shown in Fig. 5. The distortion of $\rho_{ir}^\alpha(\omega)$ for the planes in the vicinity of the interface is clearly seen. (The interface is located between the barrier plane $\alpha = 31$ and the first channel plane $\alpha = 32$.) The enhancement of the slope of the transport DOS by the Coulomb correlations has a drastic effect on the transport properties of the multilayer.

Using the fact that $\rho_{ir}^\alpha(\omega)$ is temperature-independent, except for a temperature dependent shift of the chemical potential, which we take as the origin of the energy axis, we calculate the transport function by integrating the transport function in Eq. (42). This procedure does not conserve the number of conduction electrons at each temperature and but provides, none-the-less, an insight in the effects of doping and correlation.

The temperature dependence of the electrical resistance is shown in Fig. 6 for several values of $\Delta\mu_B$ and $\Delta\mu_C$ (indicated in the figure). The resistivity drops sharply, when the chemical potential in the channel planes shifts away from the gap and cuts the upper Hubbard band. This is indicated by the dashed, dot-dashed and double-dot-dashed lines in Fig. 6 which are obtained for $\Delta\mu_C = 0.94$ (good metal), $\Delta\mu_C = 0.90$ (bad metal), $\Delta\mu_C = 0.85$ (delta-doped Mott insulator). The corresponding results for a homogeneous system exhibit the same behavior, as indicated by the full lines in Fig. 6. Note, a sharp increase in the resistance, when a bulk system is

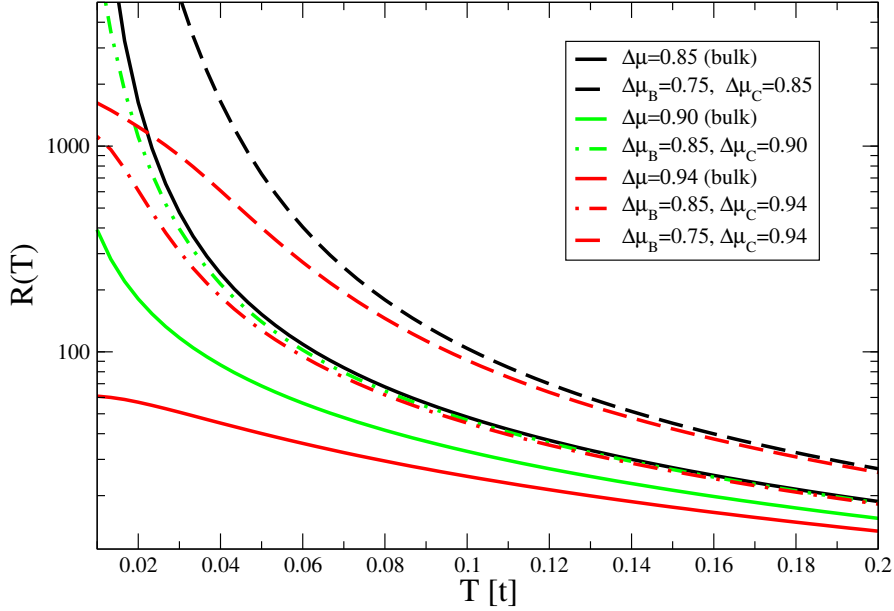


Fig. 6 (*Color online*) Electrical resistance (in arbitrary units) is plotted as a function of temperature for a multilayer with 31 planes in the barrier and 5 planes in the conducting channel. The offsets of the band centers in the barrier planes and the channel planes are indicated in the figure (nonsolid lines). The corresponding results for a homogeneous system are shown as well (solid lines).

transformed in the multilayer by an additional shift of the band-offsets in the barrier planes.

The thermopower and the effective Lorenz number of the same device are shown in Fig. 7. As expected, the thermopower increases when the electrical conductance of the system drops. Close to the metal-insulator transition, where the slope of the transport DOS at the chemical potential is very large, the thermopower of the multilayer also becomes very large. The effective Lorenz number shows large deviations from the universal value at low temperatures.

Using the same parameters as in Figs. 6 and 7 we obtain ZT which is shown in Fig. 8. Close to the metal-insulator transition, where the thermopower is large and the Lorenz number deviates from the universal value, we also find a large enhancement of the figure-of-merit, given by α^2/\mathcal{L} . Fig. 8 shows that the ZT of a multilayer (dashed and dashed-dotted lines) is smaller than the corresponding value of the bulk material with the same band-offset as used for the channel (full lines). However, the advantage of the multilayer is that the presence of the interface can impede the phonon transport and improve the overall performance of the nano-structured device with respect to the bulk.

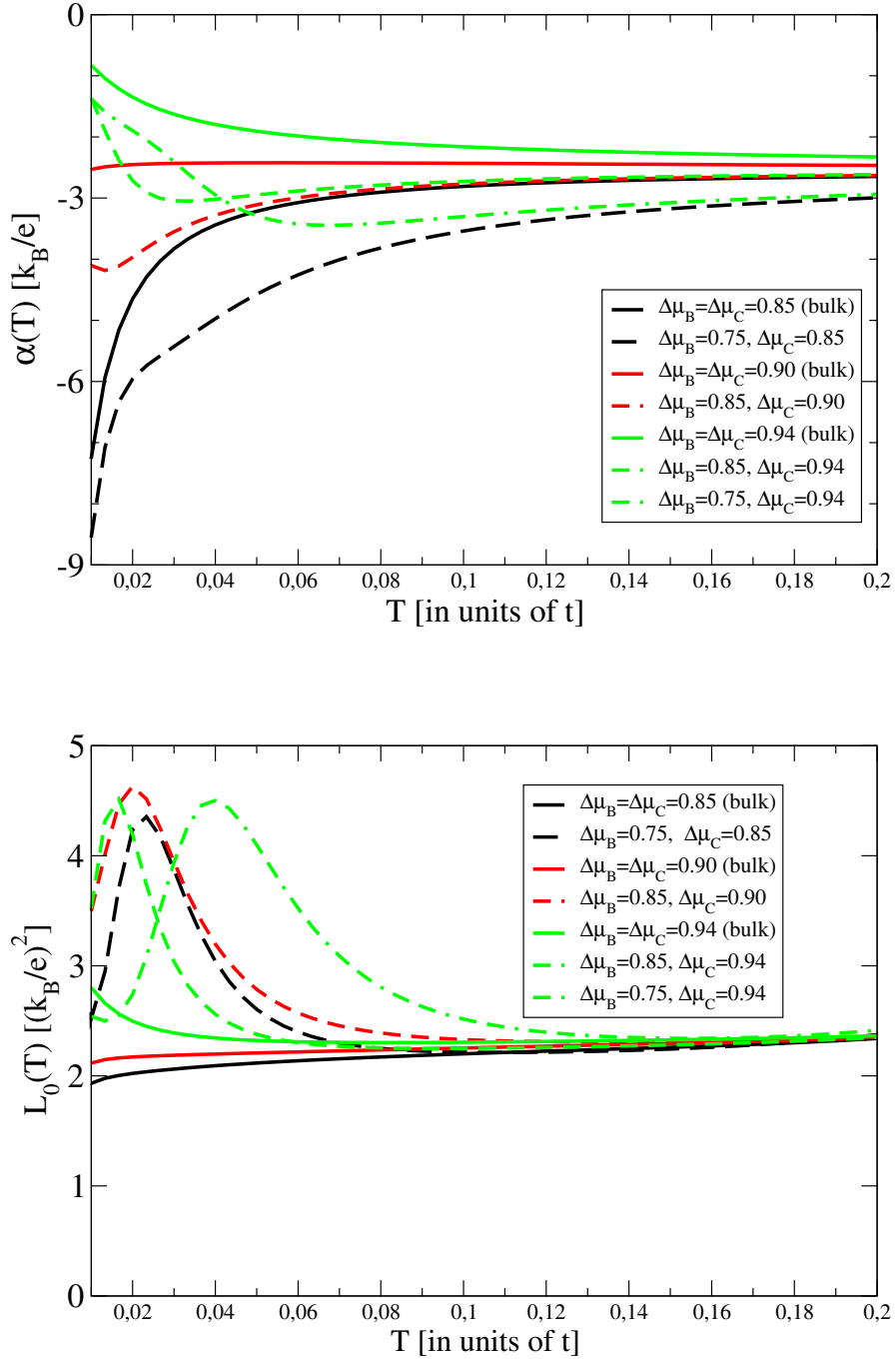


Fig. 7 (Color online) Thermopower in units of $[k_B/e]$ and the Lorenz number in units of $[k_B/e]^2$ are plotted as a function of temperature for the same parameters as in Fig. 6.

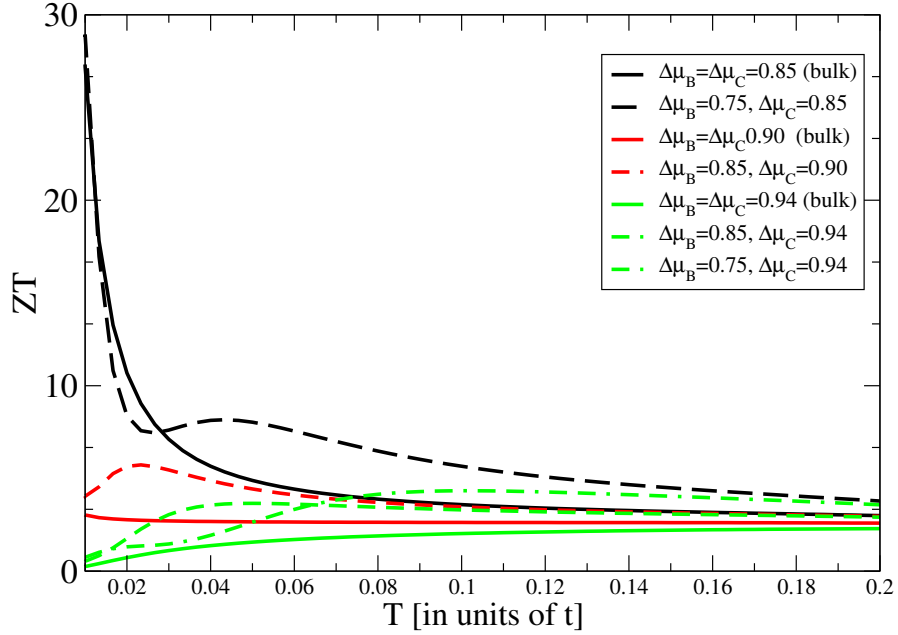


Fig. 8 (*Color online*) ZT of the device is plotted as a function of temperature for the same parameters as in Fig. 6.

10 Summary and conclusions

We presented a theory for the charge and heat transport in a multilayer consisting of several correlated metallic planes (channel) sandwiched between two semi-infinite Mott insulators (barriers). The electron dynamics of such a system is described by the Falicov-Kimball model which can be solved for large on-site correlation by the inhomogeneous DMFT. The self energy of conduction electrons has always a large imaginary part, due to the incoherent scattering on f -electrons, and the multilayer described by that model is never a Fermi liquid. The mismatch of the electronic states in the barrier and the channel planes gives rise to an electronic charge reconstruction which is most pronounced for the planes closest to the interface. We computed the heat and charge currents parallel to the interfaces by the linear response theory and found the transport coefficients of the device.

By varying the offset of the energy band in the conduction channel, we tuned the position of the chemical potential with respect to the band edge of the upper Hubbard band. For large correlation, we found the renormalized transport DOS with a large gap and, for an appropriate offset, obtained a large slope of the DOS at the chemical potential. For a delta-doped Mott insulator, i.e., for the channel planes close to the metal-insulator transition, we obtained a surprisingly large Seebeck coefficient and a much enhanced figure-of-merit. The enhancement is entirely

caused by the electron correlations and similar effects could not be found for non-interacting electrons.

Even though the purely electronic ZT is smaller in multilayers than in the bulk (computed for the bulk with the same band-offset as in the channel planes), the presence of the interfaces might impede the phonon transport in the multilayers and lead to an improved performance. For different ionic masses in the barrier and the channel planes, the scattering of phonons on the interfaces might greatly reduce the heat transport. In such a device, the proximity of the metal insulator transition might enhance the power factor and lead to ZT much larger than one.

Acknowledgements The authors want to acknowledge useful discussions with R. Monnier. This work is supported by the NSF grant No. DMR-1006605. J.K.F. is also supported by the McDevitt bequest at Georgetown University.

References

1. J. M. Luttinger, Phys. Rev. **135**, 1964, A1505.
2. Harald Boettner, Gang Chen, and Rama Venkatasubramanian, Material Research Bulletin MRS BULLETIN **31**, 211-217 (2006).
3. L. M. Falicov and J. C. Kimball, Phys. Rev. Lett. **22**, 997 (1969).
4. J. K. Freericks, *Transport in multilayered nanostructures: the dynamical mean-field theory approach*, Imperial College Press, London, 2006.
5. J. K. Freericks, Phys. Rev. B **70**, 195342 (2004); J. K. Freericks, V. Zlatić, and A. M. Shvaika, Phys. Rev. B **75**, 035133 (2007).
6. M. Jonson and G. D. Mahan, Phys. Rev. B **42**, 9350 (1990).
7. G. D. Mahan, *Many-Particle Physics*, Plenum, New York, 1981.
8. M. Potthoff and W. Nolting, Phys. Rev. B **59**, 2549 (1999).